ACS OMEGA

http://pubs.acs.org/journal/acsodf

Article

Novel Clarification of Surface Plasmon Coupling Reactions of Aromatic Alkynamine and Nitro Compounds

Yanqiu Yang, Jibiao Luo, Peng Song, Yong Ding,* and Lixin Xia*

Cite This: *ACS Omega* 2022, 7, 1165−1172

Read Online

ACCESS | Metrics & More | Article Recommendations | Supporting Information

ABSTRACT: This work presents a theoretical and experimental approach for the coupling of 4-ethynylaniline (4-APA) and 4-ethynylnitrobenzene (4-NPA) in the theoretical application of density functional theory (DFT) and experimental monitoring of surface-enhanced Raman spectroscopy (SERS). The results support electromagnetic enhancement to drive the conversion of aromatic alkynamine and nitro compounds and regulation by the catalytic coupling reaction conditions. In addition, this work investigates the adsorption site effect of surface plasmon coupling reactions of 4-APA and 4-NPA molecules into alkynyl azo compounds. This study presents theoretical and experimental images used to analyze the plasmon-driven surface catalytic reaction system.

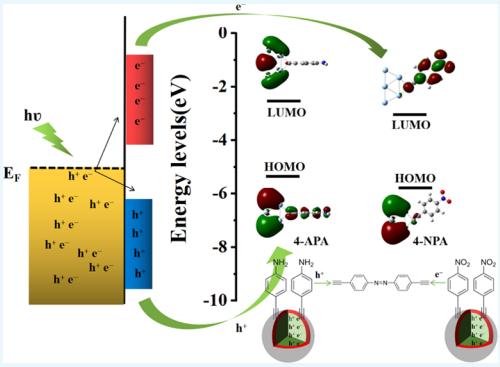

1. INTRODUCTION

Surface plasmon resonance (SPR) occurs when a laser is irradiated onto plasmonic nanostructures to make the electrons collectively oscillate at the interface with the medium and propagate along the direction of the interface.[1−5] At this time, the state of matching the characteristic frequency of the metal nanostructures with the excitation frequency can be called the coherent oscillation of surface conduction electrons.[6] If light is irradiated on the molecules adsorbed by the plasmonic metal nanostructures, charge transfer (CT) processes will occur. SPR can cause local electromagnetic field enhancement, which is an extremely important factor that greatly enhances the Raman signal due to its high throughput and low energy requirements to become the focus of research in the surface plasmon coupling reactions[7,8] and can monitor a catalytic process through surface-enhanced Raman spectroscopy (SERS).[9−13] SERS is a powerful spectral analysis technique to make up for the weak intensity of Raman spectroscopy and is widely used in biomolecular detection, food safety, clinical diagnosis, environmental testing, public safety, and medical diagnosis because it is nondestructive, applicable at low dosage, ultrasensitive, and accurate with a low detection limit as well as fingerprint recognition features.[14−18]

The typical construction of noble metal nanostructures is used as a traditional SERS substrate to enhance the signal of the probe molecules.[19−21] Therefore, the selection of target molecules on SERS substrates is extremely important, which greatly limits the use of SERS substrates. If the target molecule has a complex matrix, this will hinder its access to plasmonic nanostructures and reduce the enhancement of the Raman signal. However, if preprocessing is performed to separate the target molecules to be detected, it will be a cumbersome procedure, which violates the important performance of SERS rapid detection.[22−26] A lot of research has been undertaken to show that the aromatic compounds *p*-mercaptoaniline (PATP) and *p*-mercaptonitrobenzene (PNTP) adsorbed on plasmonic nanostructures are catalyzed into an azo material called *p*-mercaptoazobenzene (DMAB) with the aid of plasmon through plasmon-catalyzed coupling reactions.[27−30] The *p*-mercaptobenzoic acid (pMBA) molecule is selected as the probe molecule because of its prominent characteristic peaks of 1075 and 1590 cm^{-1} in SERS.[31,32] However, these model molecules are all used in the traditional sulfhydryl bonding mode, and the sulfhydryl pretreatment process for non-sulfhydryl molecules can achieve contact with traditional noble metal nanomaterials to achieve Raman signal enhancement. As a result, in addition to the complexity of this process, the number of sulfhydryl probe molecules is limited, and the application of SERS detection is further greatly restricted. Therefore, breaking the traditional sulfhydryl contact SERS detection mode, eliminating the constraints of SERS substrate selection, and exploring new nonsulfhydryl probe molecules are very critical, providing more choices for model probe molecules in the SERS field.

Received: October 14, 2021
Accepted: December 8, 2021
Published: December 21, 2021

https://doi.org/10.1021/acsomega.1c05746
ACS Omega 2022, 7, 1165−1172

In this study, the research method we applied is density functional theory (DFT) calculations[33,34] to prove experimental operations, to study the coupling reaction of 4-ethynylaniline (4-APA), and 4-nitrophenylacetylene (4-NPA) molecules. Importantly, this research avoids the traditional sulfhydryl bonding mode and uses alkynyl as the adsorption site, and adopts a combination of theory and experiment to clearly clarify the photocatalytic coupling reaction process and corresponding channel mechanism.[35] The application of noble metal silver with high catalytic performance can greatly enhance the probe molecules.[36−39] The aromatic alkyne compounds can be used as a new type of target molecule because of their simple matrix to broaden the selection range of detection molecules in SERS. In the process of exploring this type of molecular reaction and the corresponding mechanism, we studied the effect of factors such as irradiation time and power, and found that this reaction is affected by the surrounding atmosphere. The important finding is that aromatic alkyne compounds present a context of probe molecules for understanding the photocatalytic coupling reaction.

2. RESULTS AND DISCUSSION

Figure 1A shows a schematic diagram of the reaction mechanism of 4-NPA and 4-APA dimerization into *p*-alkynyl azobenzene (PAAB) driven by plasmonic nanostructures. The metal substrate is excited by a laser and decays through the surface plasmon to form hot electron and hot hole pairs to produce an enhancement in the electromagnetic field. The collective electronic transition makes the hot electrons occupy the empty state above the Fermi level, and the hot holes remain below the Fermi level. It happens that 4-APA and 4-NPA are adsorbed on the surface of metallic silver and are present around to provide corresponding orbitals for electrons and holes, so there is some possibility that there are CT processes between the surface plasmon and these two molecules. Here, the highest occupied molecular orbital (HOMO) and the lowest unoccupied molecular orbital (LUMO) belong to the frontier orbitals of the two molecules in the ground state structure optimized by calculation. It was found that the HOMO of 4-APA is 1.0 eV lower than the Fermi level of silver, which shows that it can actually be perfectly matched with the energy level of the hole.[40] The calculated LUMO energy level of 4-NPA is 1.3 eV higher than the Fermi energy level of plasmonic nanostructured silver, which also shows that it is highly consistent with the energy level of the electrons. In summary, it was observed that both the photooxidation of 4-APA and the photoreduction of 4-NPA can be completed mainly by the electromagnetic enhancement (EM) caused by SPR, which involves the assistance of these CT reactions.

Figure 1B shows the ζ potential of the plasmonic nanostructured Ag NPs and the corresponding aromatic alkyne target molecules. There is a positive charge on the outermost layer of the silver nanostructure, but it can be very easily removed. Further, in a stable state, there is an inevitable tendency to adsorb a protective agent on the surface, which makes the ζ potential value of Ag NPs become −37.1 mV. That is to say, due to the electric double layer, the number of reactive surface hydroxyls of the reducing agent sodium citrate adsorbed on the surface of the Ag NPs are negatively charged. The 4-NPA molecule ionizes in the solution to form the 4-NPA anion, which produces a negative charge (−3.38 mV) for

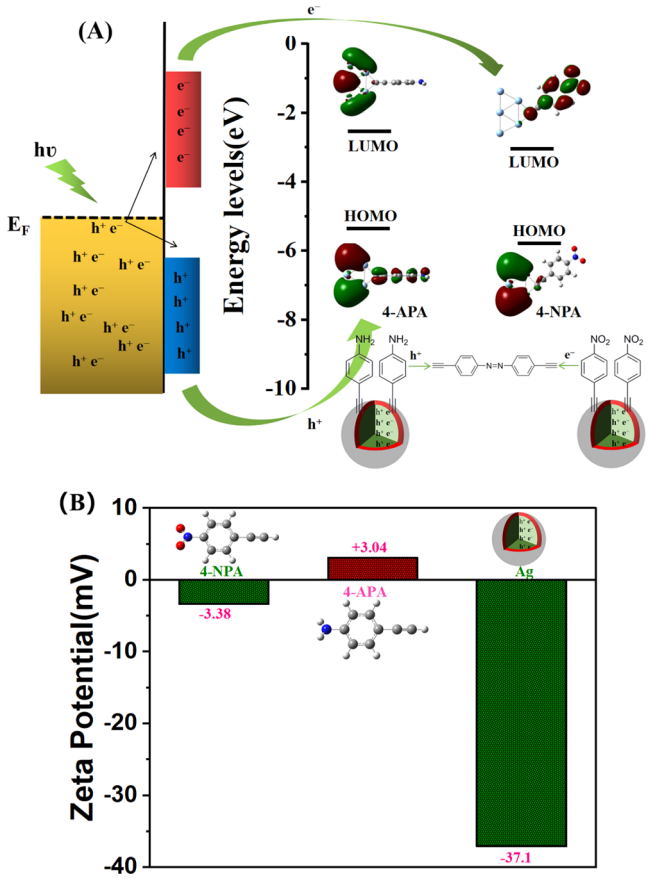

Figure 1. (A) Schematic diagram of the reaction mechanism of 4-NPA and 4-APA dimerization into PAAB driven by plasmonic nanostructures. The metal substrate generates electron−hole pairs after being irradiated with laser light. Frontier molecular orbital energy level diagrams of 4-NPA and 4-APA on the Ag_5 cluster, red represents electrons and green represents holes. (B) The ζ potential of the plasmonic nanostructured Ag NPs and the corresponding aromatic alkynes target molecules.

the solution. Similarly, the 4-APA molecule ionizes in the solution to form the 4-APA cation that is positively charged (+3.04 mV). And the ζ potential curves with standard deviations of 4-NPA, 4-APA, and the plasmonic nanostructured Ag NPs show the potential trend in detail, and this standard deviation shows the accuracy and stability of the potential value (as shown in Figure S1A−C of the Supporting Information). Importantly, the potentials of 4-NPA and 4-APA are relatively low, so the interaction between the two molecules and the Ag NPs is not completed by an electrostatic interaction mechanism.

In the SEM image (shown in Figure S2 of the Supporting Information), it can be seen that the surface morphology of the Ag NPs is mainly spherical, with a little rod-like appearance and the size of the nanostructure is about 50 nm. And these Ag NPs exhibit a rough surface, which can generate a large number of hot spots and promote surface plasmon coupling reactions of aromatic alkynamine and nitro compounds. In the following experiments, the investigation and analysis of the interaction between the silver metal nanostructure and 4-NPA and 4-APA molecules are observed in the UV−vis spectrum. First, we obtained Ag NPs by the traditional sodium citrate reduction method, which is equivalent to the Ag_5 clusters in the DFT theoretical simulation, and then formed homoge-

https://doi.org/10.1021/acsomega.1c05746
ACS Omega 2022, 7, 1165−1172

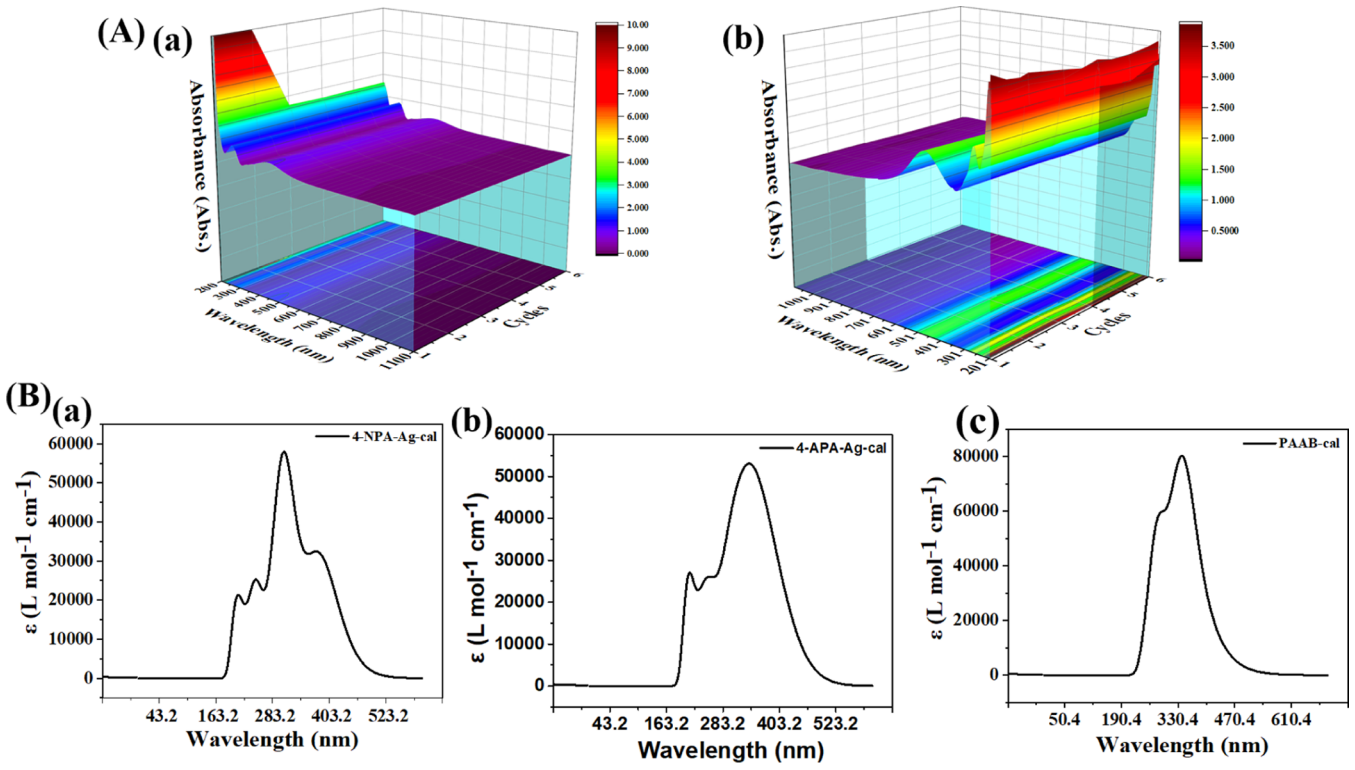

Figure 2. (A) Experimental interactions between the silver metal nanostructure and 4-NPA (a) and 4-APA (b) molecules are shown in the UV−vis spectrum. (B) The simulated UV−vis absorption spectrum was calculated by DFT for Ag_5 clusters and their complexes with 4-NPA (a) and 4-APA (b) molecules, and the product PAAB was generated (c).

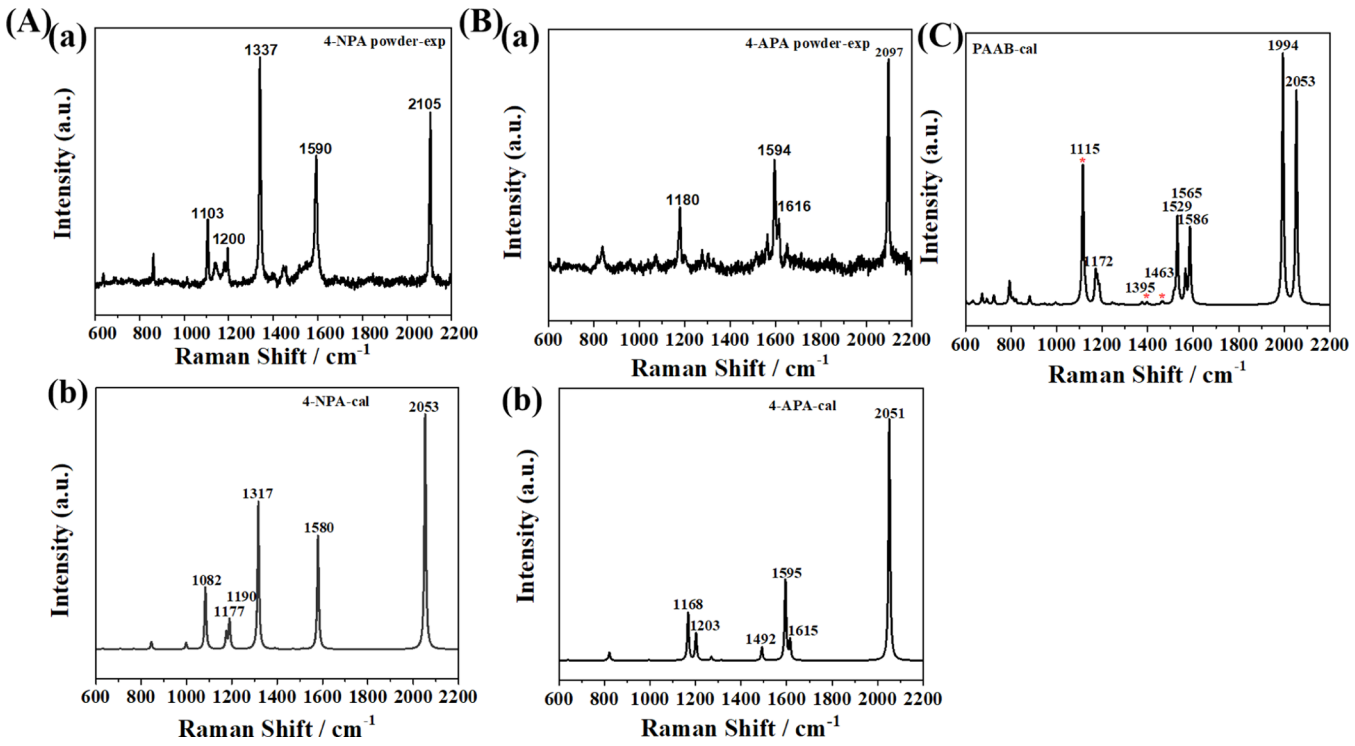

Figure 3. (A) Normal Raman spectra (NRS) of 4-NPA molecules through the experiment (a) and DFT theoretical simulation calculations (b). (B) Raman spectrum of the 4-APA molecule in the experiment (a) and calculation (b). (C) Theoretically simulated SERS spectrum of the product formed by the combination of alkynyl aromatic compound and Ag_5 cluster excited by a 532 nm laser.

neous mixtures with 4-NPA and 4-APA molecular solutions to perform the ultraviolet absorption investigation experiment. Figure 2Aa shows that the characteristic absorption peak of Ag NPs appeared in the experiment at 460 nm, and the absorption peak at around 280 nm was attributed to the characteristic peak of 4-NPA molecules. However, in Figure 2Ab, we can see

https://doi.org/10.1021/acsomega.1c05746
ACS Omega 2022, 7, 1165−1172

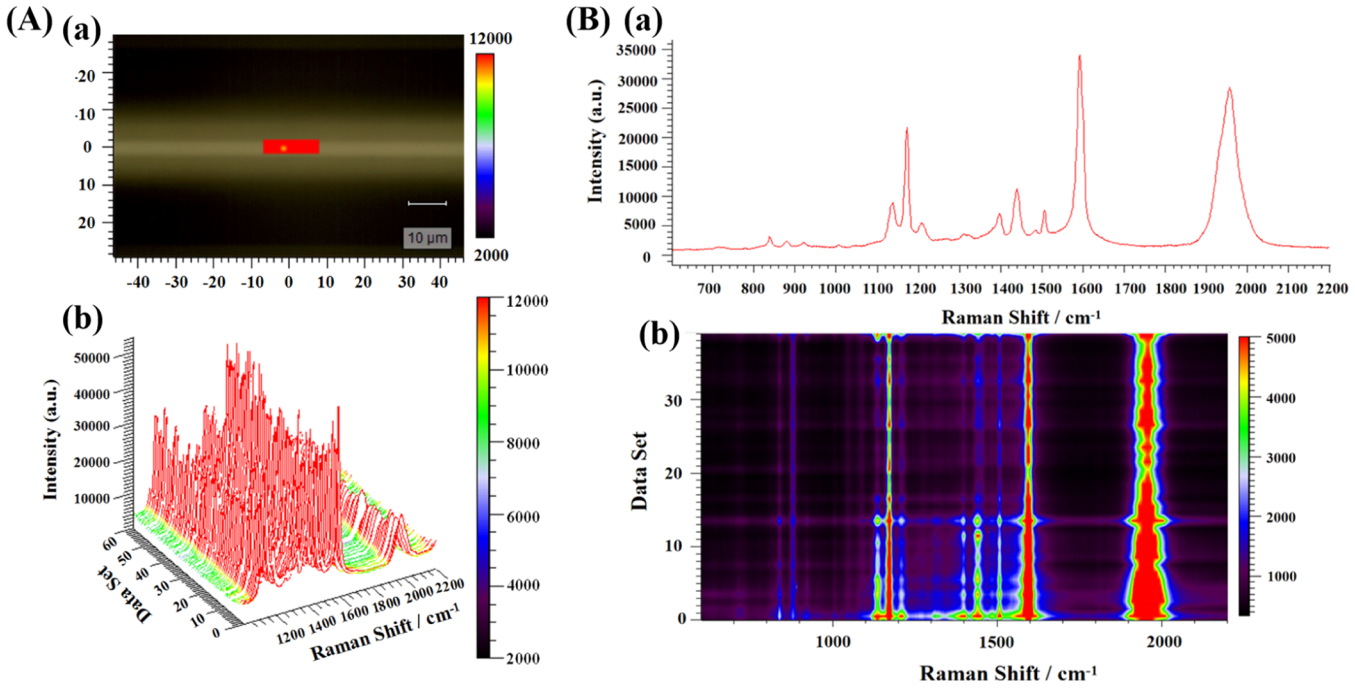

Figure 4. (A) Mapping results of 4-NPA−Ag NPs. (a) Selected area under the microscope. (b) View of the original data in the 3-D image based on the vibrational band at 1436 cm^{-1}, red. (B) Mapping results of 4-APA−Ag NPs. (a) The SERS spectrum of a randomly selected point is among many mapping points. (b) The corresponding 2-D SERS spectrum under laser excitation at 532 nm.

that the characteristic absorption peak for the probe molecule 4-APA caused using the same Ag NPs in the experiment is around 450 nm, and the characteristic peak is around 260 nm identified as the characteristic absorption peak of 4-APA molecules.

The simulated UV−vis absorption spectra were calculated using DFT for Ag_5 clusters and their complexes with 4-NPA and 4-APA molecules are shown in Figure 2Ba and b, respectively, and the product PAAB generated is shown in Figure 2Bc. Through the simulated UV−vis spectrum, the interaction between the alkynyl molecules of 4-NPA and 4-APA and the Ag_5 cluster was studied in detail, which is used to prove the absorption phenomenon in the experiment. It can be seen that the Ag_5 cluster shows a very strong absorption peak near 320 nm, which is similar to other Ag clusters such as Ag_{20} studied previously,[41] and its shoulder peak appears near 380 nm. It can be found that the small silver clusters of Ag_5 in the theoretical simulation and the characteristic absorption peaks of the Ag NPs synthesized through experiments are still different, but it can be emphasized that both have some effect on the studied aromatic alkyne compounds. What can be concluded here is that the maximum excitation near these two absorption peaks is related to SPR, indicating that this small Ag_5 metal cluster can be used as a model system for understanding the excitation of surface plasmons. It can also be seen that in addition to the characteristic absorption peaks of the Ag_5 clusters, the same peaks of 4-NPA are seen at 240 and 270 nm, and it is determined that this system is a composite system of 4-NPA and Ag_5 clusters from Figure 2Ba. In Figure 2Bb, it can be found that when 4-APA molecules interact with Ag_5 clusters, only the maximum absorption peak of Ag_5 appears near 340 nm. Different probe molecules have different functional groups in the system, resulting in inconsistency in the positions of the Ag_5 absorption peaks in the two alkynyl aromatic hydrocarbon molecular systems. In addition, the characteristic absorption peak of the 4-APA probe molecules can be observed near 210 and 250 nm and it can be concluded that the 4-APA probe molecule is complexed with the Ag_5 cluster. In Figure 2Bc, it can be seen that the absorption peaks of Ag_5 clusters and probe molecules appear at 340 and 284 nm, respectively, but at this time, it can be preliminarily judged that alkynyl aromatic compounds have new molecular formulation under the action of silver clusters. In the UV−vis spectrum, the interaction between alkynyl aromatic compounds and metal nanostructures has been fully analyzed through the experiment and theoretical simulation calculation verification. This silver nanostructure has a certain enhancement effect on aromatic alkyne compounds.

The certain enhancement effect of plasmonic silver metal nanostructure on alkynyl aromatic compounds has been initially explained. However, the specific mode of action and the result and process of the enhancement are not clear, but this phenomenon can be further analyzed using SERS and the vibration frequency displacement is clearly seen. Normal Raman spectra (NRS) of 4-NPA molecules are shown in Figure 3A through experiment (Figure 3Aa) and a DFT theoretical simulation calculation (Figure 3Ab). The calculated Raman shift of 4-NPA is compared with the experimental data (2105 cm^{-1}) and a large blue shift in the Raman quiet zone (2053 cm^{-1}) is observed, both of which represent the vibration frequency of the C≡C bond.[42] The peak at 1317 cm^{-1} is calculated, and in the experiment (1337 cm^{-1}) is assigned to the typical peak of the nitro (ν_{NO_2}) group in 4-NPA.[43] The Raman peaks at 1082, 1177, and 1190 cm^{-1} were calculated by simulation and the peaks at around 1200 and 1103 cm^{-1} in the experiment are attributed to the C−H in-plane bending. Although there are slight displacement differences in experiments and calculations, they all represent the same vibration mode, and the Raman peak of 1597 cm^{-1} is due to the C−C stretching modes of the aromatic ring.[44] The calculations based

https://doi.org/10.1021/acsomega.1c05746
ACS Omega 2022, 7, 1165−1172

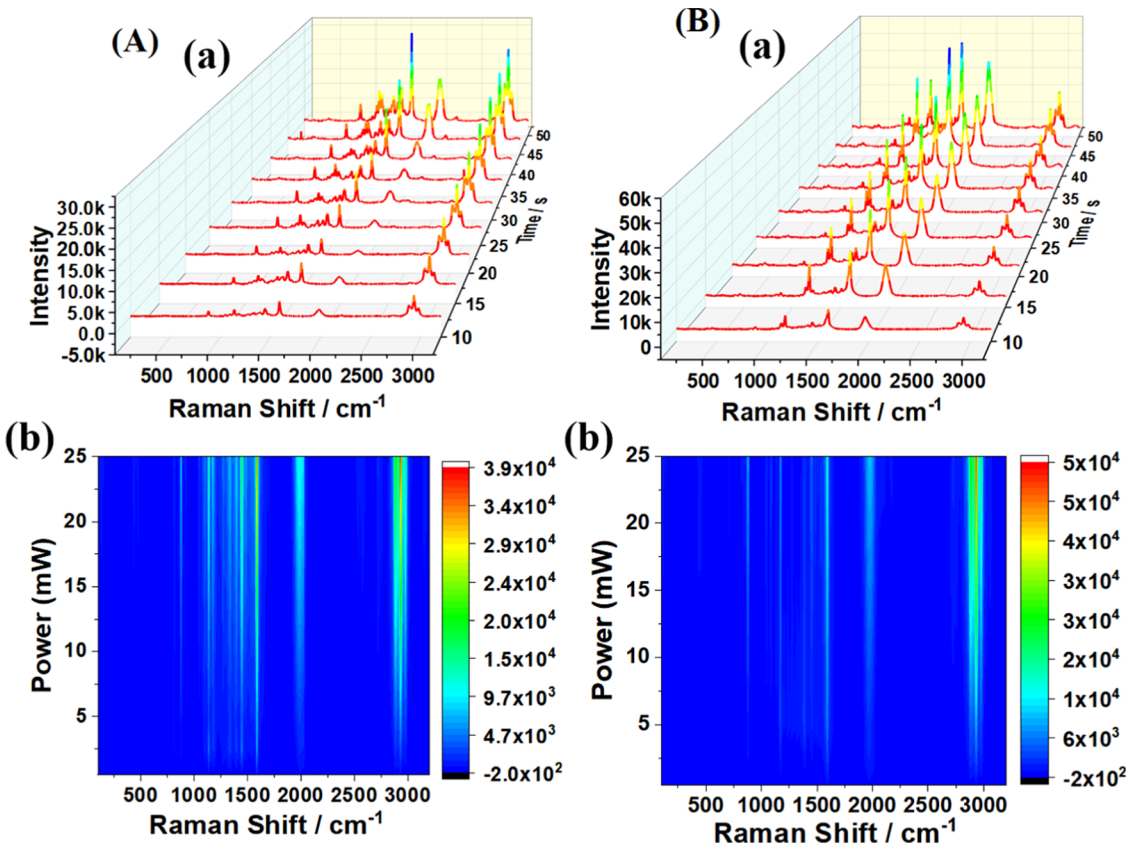

Figure 5. (A) Time-dependent (a) and laser power-dependent (b) SERS spectra of 4-NPA−Ag NPs. (B) The time-dependent (a) and laser power-dependent (b) SERS spectra of 4-APA−Ag NPs.

on the above provide a theoretical explanation for the experimental Raman spectroscopic behavior of 4-NPA molecules.

Figure 3B shows the Raman spectrum of the 4-APA molecule obtained by experiment (Figure 3Ba) and calculation (Figure 3Bb). Similarly, in the vibration modes of this molecule, the characteristic vibration peak of the alkynyl group can be clearly observed, which is similar to that of the 4-NPA molecule. More importantly, the characteristic peak of the amino (ν_{NH2}) groups is clearly seen at 1610 cm^{-1}.[45] Obviously, the strong characteristic peak seen at 1595 cm^{-1} obtained by calculation and 1594 cm^{-1} in the experiment is related to the C−C vibrational modes of the aromatic ring, and the Raman vibration peak near 1180 cm^{-1} is due to C−H bending in 4-APA. The simulated Raman spectrum is consistent with the experimental spectrum using a 532 nm laser at 2.5 mW continuously irradiated for 10 s on 4-NPA and 4-APA molecules. The theoretically simulated SERS spectrum of the product formed by the combination of alkynyl aromatic compound and Ag_5 cluster excited by a 532 nm laser is shown in Figure 3C. The obvious split peaks of 1994 and 2053 cm^{-1} of the C≡C region are worth noting when the aromatic molecules with alkynyl groups interact with the metal interface. Specifically, the alkynyl aromatic molecules 4-NPA and 4-APA are bonded to the metal nanostructure through the alkynyl carbon. In addition, it can be seen that there is a certain vibration frequency shift at 1115 cm^{-1} and weak bands at 1395 and 1463 cm^{-1} corresponding to the −N═N− bond, so it can be concluded that alkynyl aromatic molecules are converted into PAAB driven by plasmons.

After determining the band assignment by DFT simulation, to prove our hypothesis further, the plasmon-driven catalytic reaction of the complex of 4-NPA and 4-APA probe molecules with Ag NPs was monitored by in situ SERS mapping technology using a 532 nm laser wavelength and 2.5 mW laser power (in the experiment). Figure 4A, from top to bottom, shows a random selection of a specific area to be tested to obtain a rainbow image (Figure 4Aa) and shows original data in a 3-D SERS image (Figure 4Ab) under a microscope for 4-NPA, the mapping data are based on the vibrational mode at 1436 cm^{-1}. We can see that almost all the selected areas of 4-NPA−Ag NPs are red, indicating that the reaction has proceeded relatively adequately. The 3-D SERS spectrum of this system has characteristic peaks at 1142, 1398, and 1436 cm^{-1} that are clearly assigned to the −N═N− bond. In addition, there is a deviation of the Raman characteristic peak of the C≡C stretching vibration at 2067 cm^{-1} relative to the actual position of the powder state, and then all these data are combined and analyzed, which ideally proves the formation of a new compound, PAAB.

Figure 4B shows the curve relationship diagram (Figure 4Ba) and the corresponding 2-D SERS spectrum (Figure 4Bb) for the 4-APA−Ag NP composite system obtained using mapping technology. The N═N characteristic vibration frequency peaks at 1152, 1397, and 1439 cm^{-1} and the C≡C vibration peaks at 1961 cm^{-1} in the upper and lower figures correspond one-to-one to complement each other from the angle of the curve and the color area. This proves that 4-APA target molecules are successfully transformed into PAAB molecules under the action of Ag NPs and have relatively high chemical reactivity. The application of this mapping

https://doi.org/10.1021/acsomega.1c05746
ACS Omega 2022, 7, 1165−1172

technology not only verifies that alkynyl aromatic molecules are driven by a plasmonic metal substrate but also avoids the contingency of data results and shows the excellent characteristics of the uniformity and repeatability of the system.

To completely monitor the plasmon-catalyzed coupling reaction process of alkynyl aromatic compounds further, the influence of the input time and energy was also studied (Figure 5). In the composite system of 4-NPA−Ag NPs (Figure 5Aa), as the illumination time under 532 nm laser excitation was prolonged, significant band splitting occurred for ν_s(C≡C) at 2211 and 1985 cm^{-1}, the splitting of the peak is considered to be caused by a small amount of polymer. In the 4-APA−Ag NP (Figure 5Ba) composite system, the characteristic vibration peak of ν_s(C≡C) observed at 1965 cm^{-1} is blue-shifted a lot compared with the peak position in the powder. At the same time, when the laser irradiation time is extended, we also observe that the three vibration mode peaks of N═N gradually become stronger within a certain laser intensity. Other characteristic vibration peaks of C−H and C−C also tend to increase in intensity in the composite 4-NPA−Ag NP and 4-APA−Ag NP systems. This also illustrates the relationship between the intensity of each characteristic peak and the laser power in Figure 5Ab,Bb. From 5 to 25 mW, the characteristic peak intensities of C≡C, N═N, and C−C and C−H of the aromatic ring increase and reach a maximum value at 25 mW. Increasing the power too much damages the sample, here the power was varied to 25 mW. For exploring the period of laser irradiation time and power increase, alkynyl aromatic molecules were adsorbed onto Ag NPs through alkyne functional groups, and 4-NPA and 4-APA molecules were converted to PAAB on the surface of the Ag NPs driven by surface plasmons. Gradually, with the increase of laser power and time, a larger electromagnetic field can be generated on the surface of metallic Ag NPs, leading to further enhancement of this catalytic reaction.

3. CONCLUSIONS

This research has achieved the expected goals to a certain extent. It has deepened the understanding of selective catalytic coupling reactions on metal nanostructures and, more importantly, broadened the selection of probe molecules based on the traditional sulfhydryl bonding mode adding alkynyl aromatic model probe molecules in SERS. Through the analysis of the alkynyl vibration frequency shifts and the comparison of the peak intensities, the important adsorption site was determined through DFT calculation and experimental SERS monitoring, and the alkynyl carbon is bonded to the SERS-enhanced substrate. The conversion product of these alkynyl aromatic molecules was confirmed to be experimentally driven by plasmons on a metal substrate. The key point is that in the process of molecular transformation, there is a detailed analysis of the reaction mechanism for the presence of CT Raman enhancement under the main EM enhancement mechanism. Based on the above, we have studied the environmental impact of the selective catalysis coupling reactions of 4-NPA and 4-APA molecules when interacting with metal clusters and show that it depends on the irradiation time and irradiation power. This work expands the strategy through the elaboration of the mechanism regarding the selective conversion of alkynyl aromatic compounds driven by plasmons on the surface of metal nanostructures.

4. EXPERIMENTAL AND COMPUTATIONAL METHODS

4.1. Calculation. In the theoretical DFT calculations, Ag_5 metal clusters were used to simulate the SERS substrate to investigate the bonding mode, adsorption configuration, and the corresponding SERS spectra of 4-APA and 4-NPA. The localized SPR induced electric field of silver nanoparticles (Ag NPs) was stimulated under an incident laser at 532 nm. Combining the calculation of the vibration frequency and intensity of free molecules, a detailed study was performed on the frequency shift under the enhancement of the Ag_5 cluster. The B3LYP functional and 6−31G(d) basis set were used to optimize the ground state geometric configuration of C, H, O, and N atoms in the 4-APA and 4-NPA molecules, and the ground state Ag atoms were calculated using the LANL2DZ method for optimization. The abovementioned quantitative calculations are based on the Gaussian 09 D01 software package for theoretical calculations. In addition, to achieve a better agreement between the theoretical calculation frequency and the experimental vibration frequency, calculation data such as Raman and SERS spectra were obtained using the Multiwfn 3.6 program. The calculation of the vibrational frequencies of all structures was performed without the imaginary frequency.

4.2. Experimental Characterization. The Raman and SERS spectra of the samples were obtained using a Renishaw InVia Reflex spectrometer with a 532 nm light source. Ultraviolet−visible (UV−vis) spectra of the Ag NPs formed using the sodium citrate reduction method and the mixed system of 4-APA−Ag NPs and 4-NPA−Ag NPs were obtained using a Perkin Elmer Lambda 35 spectrophotometer (Norwalk, CT). ζ Potential measurements of probe molecules and Ag NPs materials were obtained using a Zetasizer Nano-ZS particle analyzer (Malvern Corp., England).

■ ASSOCIATED CONTENT

Supporting Information

The Supporting Information is available free of charge at https://pubs.acs.org/doi/10.1021/acsomega.1c05746.

ζ Potential curves with standard deviation and SEM image, as well as some figures (S1−S2) related to this manuscript (PDF)

■ AUTHOR INFORMATION

Corresponding Authors

Yong Ding − *Department of Physics, Liaoning University, Shenyang 110036, P. R. China*; Email: dingyong@lnu.edu.cn

Lixin Xia − *Department of Chemistry, Liaoning University, Shenyang 110036, P. R. China; Yingkou Institute of Technology, Yingkou 115014, P. R. China*; Email: lixinxia@lnu.edu.cn

Authors

Yanqiu Yang − *Department of Physics, Liaoning University, Shenyang 110036, P. R. China*

Jibiao Luo − *Department of Physics, Liaoning University, Shenyang 110036, P. R. China*

Peng Song − *Department of Physics, Liaoning University, Shenyang 110036, P. R. China*; orcid.org/0000-0003-3093-0068

Complete contact information is available at: https://pubs.acs.org/10.1021/acsomega.1c05746

Notes

The authors declare no competing financial interest.

■ ACKNOWLEDGMENTS

This work was supported by the National Natural Science Foundation of China (Grant Nos. 11974152 and 21671089), the LiaoNing Revitalization Talents Program (Grant No. XLYC1807162), the Shenyang Highlevel Innovative Talents Program (RC200565), the Scientific Research Projects of Liaoning Provincial Department of Education (L2020002), the Liaoning Provincial Natural Science Foundation Joint Fund Project (2020-YKLH-22), the Science program of Liaoning Provincial Department of Education (LJKZ0097), the Intercollegiate Cooperation Project of Colleges and Universities of Liaoning Provincial Department of Education.

■ REFERENCES

(1) Ding, S. Y.; You, E. M.; Tian, Z. Q.; Moskovits, M. Electromagnetic theories of surface-enhanced Raman spectroscopy. *Chem. Soc. Rev.* **2017**, *46*, 4042−4076.
(2) Xie, W.; Schlucker, S. Hot electron-induced reduction of small molecules on photorecycling metal surfaces. *Nat. Commun.* **2015**, *6*, No. 7570.
(3) Zaleski, S.; Wilson, A. J.; Mattei, M.; Chen, X.; Goubert, G.; Cardinal, M. F.; Willets, K. A.; Van Duyne, R. P. Investigating Nanoscale Electrochemistry with Surface- and Tip-Enhanced Raman Spectroscopy. *Acc. Chem. Res.* **2016**, *49*, 2023−2030.
(4) Zhang, X.; Chen, Y. L.; Liu, R. S.; Tsai, D. P. Plasmonic Photocatalysis. *Rep. Prog. Phys.* **2013**, *76*, No. 046401.
(5) Linic, S.; Christopher, P.; Ingram, D. B. Plasmonic-metal nanostructures for efficient conversion of solar to chemical energy. *Nat. Mater.* **2011**, *10*, 911−921.
(6) Watanabe, K.; Menzel, D.; Nilius, N.; Freund, H. J. Photochemistry on Metal Nanoparticles. *Chem. Rev.* **2006**, *106*, 4301−4320.
(7) Cui, L.; Ren, X.; Yang, X. Z.; Wang, P. J.; Qu, Y. Q.; Liang, W. J.; Sun, M. T. Plasmon-driven catalysis in aqueous solutions probed by SERS spectroscopy. *J. Raman Spectrosc.* **2016**, *47*, 877−883.
(8) Lin, W. H.; Cao, Y. Q.; Wang, P. J.; Sun, M. T. Unified treatment for plasmon-exciton co-driven reduction and oxidation reactions. *Langmuir* **2017**, *33*, 12102−12107.
(9) Demirel, G.; Usta, H.; Yilmaz, M.; Celik, M.; Alidagi, H. A.; Buyukserin, F. Surface-enhanced Raman spectroscopy (SERS): an adventure from plasmonic metals to organic semiconductors as SERS platforms. *J. Mater. Chem. C* **2018**, *6*, 5314−5335.
(10) Fang, Y. R.; Zhang, Z. L.; Sun, M. T. High vacuum tip-enhanced Raman spectroscope based on a scanning tunneling microscope. *Rev. Sci. Instrum.* **2016**, *87*, No. 033104.
(11) Lee, M.; Lee, K.; Kim, K. H.; Oh, K. W.; Choo, J. SERS-based immunoassay using a gold array-embedded gradient microfluidic chip. *Lab Chip* **2012**, *12*, 3720−3727.
(12) Kanipe, K. N.; Chidester, P. P. F.; Stucky, G. D.; Moskovits, M. Large format surface-enhanced Raman spectroscopy substrate optimized for enhancement and uniformity. *ACS Nano* **2016**, *10*, 7566−7571.
(13) Zheng, Y.; Wang, A.; Wang, Z.; Fu, L.; Peng, F. Facial synthesis of carrageenan/reduced graphene oxide/Ag composite as efficient SERS platform. *Mat. Res.* **2017**, *20*, 15−20.
(14) Han, X. X.; Huang, G. G.; Zhao, B.; Ozaki, Y. Label-free highly sensitive detection of proteins in aqueous solutions using surface-enhanced Raman scattering. *Anal. Chem.* **2009**, *81*, 3329−3333.
(15) Pieczonka, N. P.; Aroca, R. F. Single molecule analysis by surfaced-enhanced Raman scattering. *Chem. Soc. Rev.* **2008**, *37*, 946−954.
(16) Quiroz, A.; Sato-Berrú, R.; Massoni, E.; Sánchez, R.; Bañuelos-Muñeton, J. G.; Sánchez-Flores, N. A.; Guerra, J. A.; Grieseler, R. Silver/palladium nanofilms for SERS application: Obtention and characterization. *Mater. Chem. Phys.* **2021**, *273*, No. 125065.
(17) Zhang, C.-Y.; Hao, R.; Zhao, B.; Hao, Y.-W.; Liu, Y.-Q. A ternary functional Ag@GO@Au sandwiched hybrid as an ultra-sensitive and stable surface enhanced Raman scattering platform. *Appl. Surf. Sci.* **2017**, *409*, 306−313.
(18) Ni, Z. H.; Chen, W.; Fan, X. F.; Kuo, J. L.; Yu, T.; Wee, A. T. S.; Shen, Z. X. Raman spectroscopy of epitaxial graphene on a SiC substrate. *Phys. Rev. B* **2008**, *77*, No. 115416.
(19) Zheng, Z.; Tachikawa, T.; Majima, T. Plasmon-enhanced formic acid dehydrogenation using anisotropic Pd-Au nanorods studied at the single-particle level. *J. Am. Chem. Soc.* **2015**, *137*, 948−957.
(20) Zhang, Z. L.; Xu, P.; Yang, X. Z.; Liang, W. J.; Sun, M. T. Surface plasmon-driven photocatalysis in ambient, aqueous and high-vacuum monitored by SERS and TERS. *J. Photochem. Photobiol., C* **2016**, *27*, 100−112.
(21) Xie, W.; Walkenfort, B.; Schlucker, S. Label-free SERS monitoring of chemical reactions catalyzed by small gold nanoparticles using 3D plasmonic superstructures. *J. Am. Chem. Soc.* **2013**, *135*, 1657−1660.
(22) Guselnikova, O.; Postnikov, P.; Chehimi, M. M.; Kalachyovaa, Y.; Svorcik, V.; Lyutakov, O. Surface plasmon-polariton: A novel way to initiate azide-alkyne cycloaddition. *Langmuir* **2019**, *35*, 2023−2032.
(23) Wu, T.; Fitchett, C. M.; Brooksby, P. A.; Downard, A. J. Building tailored interfaces through covalent coupling reactions at layers grafted from aryldiazonium salts. *ACS Appl. Mater. Interfaces* **2021**, *13*, 11545−11570.
(24) Choudhary, P.; Sen, A.; Kumar, A.; Dhingra, S.; Nagaraja, C. M.; Krishnan, V. Sulfonic acid functionalized graphitic carbon nitride as solid acid−base bifunctional catalyst for Knoevenagel condensation and multicomponent tandem reactions. *Mater. Chem. Front.* **2021**, *5*, 6265−6278.
(25) Choudhary, P.; Bahuguna, A.; Kumar, A.; Dhankhar, S. S.; Nagaraja, C. M.; Krishnan, V. Oxidized graphitic carbon nitride as a sustainable metal-free catalyst for hydrogen transfer reactions under mild conditions. *Green Chem.* **2020**, *22*, 5084−5095.
(26) Wang, L. P.; Mo, J. L.; Xia, Y. H.; Lu, T.; Jin, Y.; Peng, Y.; Zhang, L. Y.; Tang, Y. L.; Du, S. H. Monitoring allergic reaction to penicillin based on ultrasensitive detection of penicilloyl protein using alkyne response SERS immunosensor. *J. Pharm. Biomed. Anal.* **2021**, *206*, No. 114377.
(27) Fang, Y. R.; Li, Y. Z.; Xu, H. X.; Sun, M. T. Ascertaining p,p′-dimercaptoazobenzene produced from p-aminothiophenol by selective catalytic coupling reaction on silver nanoparticles. *Langmuir* **2010**, *26*, 7737−7746.
(28) Huang, Y. Z.; Fang, Y. R.; Yang, Z. L.; Sun, M. T. Can p, p′-Dimercaptoazobisbenzene be produced from p-Aminothiophenol by surface photochemistry reaction in the junctions of a Ag nanoparticle−molecule−Ag (or Au) film. *J. Phys. Chem. C* **2010**, *114*, 18263−18269.
(29) Tang, X. H.; Cai, W. Y.; Yang, L. B.; Liu, J. H. Monitoring plasmon-driven surface catalyzed reactions in situ using time-dependent surface-enhanced Raman spectroscopy on single particles of hierarchical peony-like silver microflowers. *Nanoscale* **2014**, *6*, 8612−8616.
(30) Lin, W. H.; Cao, E.; Zhang, L. Q.; Xu, X. F.; Song, Y. Z.; Liang, W. J.; Sun, M. T. Electrically enhanced hot hole driven oxidation catalysis at the interface of a plasmon-exciton hybrid. *Nanoscale* **2018**, *10*, 5482−5488.
(31) Yang, Y. Q.; Zhang, H. R.; Ma, L. P.; Lu, X. M.; Wu, S. W.; Song, P.; Xia, L. X. The efficient ionization reaction of DTBA achieved by surface plasmon catalysis effect. *Plasmonics* **2020**, *15*, 1525−1532.
(32) Yang, Y. Q.; Lu, X. M.; Gao, C.; Wu, S. W.; Song, P.; Xia, L. X. Surface plasmon-induced hot electrons as the racemate to regulate ionization. *J. Phys. Chem. C* **2021**, *125*, 757−764.

https://doi.org/10.1021/acsomega.1c05746
ACS Omega 2022, 7, 1165−1172

(33) Marenich, A. V.; Cramer, C. J.; Truhlar, D. G. Universal solvation model based on solute electron density and on a continuum model of the solvent defifined by the bulk dielectric constant and atomic surface tensions. *J. Phys. Chem. B* **2009**, *113*, 6378−6396.
(34) Jiang, R.; Zhang, M.; Qian, S.-L.; Yan, F.; Pei, L.-Q.; Jin, S.; Zhao, L.-B.; Wu, D.-Y.; Tian, Z.-Q. Photoinduced surface catalytic coupling reactions of aminothiophenol derivatives investigated by SERS and DFT. *J. Phys. Chem. C* **2016**, *120*, 16427−16436.
(35) Xu, H. X.; Käll, M. Surface-plasmon-enhanced optical forces in silver nanoaggregates. *Phys. Rev. Lett.* **2002**, *89*, No. 246802.
(36) Chen, X. W.; Peng, M.; Cai, X. B.; Chen, Y. L.; Jia, Z. M.; Deng, Y. C.; Mei, B. B.; Jiang, Z.; Xiao, D. Q.; Wen, X. D.; Wang, N.; Liu, H. Y.; Ma, D. Regulating coordination number in atomically dispersed Pt species on defect-rich graphene for n-butane dehydrogenation reaction. *Nat. Commun.* **2021**, *12*, No. 2664.
(37) Huang, F.; Deng, Y. C.; Chen, Y. L.; Cai, X. B.; Peng, M.; Jia, Z. M.; Xie, J. L.; Xiao, D. Q.; Wen, X. D.; Wang, N.; Jiang, Z.; Liu, H. Y.; Ma, D. Anchoring Cu_1 species over nanodiamond-graphene for semi-hydrogenation of acetylene. *Nat. Commun.* **2019**, *10*, No. 4431.
(38) Liu, H. Y.; Zhang, L. Y.; Wang, N.; Su, D. S. Palladium nanoparticles embedded in the inner surfaces of carbon nanotubes: synthesis, catalytic activity, and sinter resistance. *Angew. Chem., Int. Ed.* **2014**, *53*, 12634−12638.
(39) Huang, F.; Deng, Y. C.; Chen, Y. L.; Cai, X. B.; Peng, M.; Jia, Z. M.; Ren, P. J.; Xiao, D. Q.; Wen, X. D.; Wang, N.; Liu, H. Y.; Ma, D. Atomically dispersed Pd on nanodiamond/graphene hybrid for selective hydrogenation of acetylene. *J. Am. Chem. Soc.* **2018**, *140*, 13142−13146.
(40) Zhao, L. B.; Zhang, M.; Huang, Y. F.; Williams, C. T.; Wu, D. Y.; Ren, B.; Tian, Z. Q. Theoretical study of plasmon-enhanced surface catalytic coupling reactions of aromatic amines and nitro compounds. *J. Phys. Chem. Lett.* **2014**, *5*, 1259−1266.
(41) Zhao, L. L.; Jensen, L.; Schatz, G. C. Pyridine−Ag_{20} Cluster: A model system for studying surface-enhanced Raman scattering. *J. Am. Chem. Soc.* **2006**, *128*, 2911−2919.
(42) Wang, J.; Dong, J.-C.; Yang, J.; Wang, Y.; Zhang, C.-J.; Xu, M.-M.; Mao, B.-W.; Yao, J.-L.; Li, J.-F.; Tian, Z.-Q. In situ SERS and SHINERS study of electrochemical hydrogenation of p-ethynylaniline in nonaqueous solvents. *Electrochem. Commun.* **2017**, *78*, 16−20.
(43) Meng, M.; Fang, Z. C.; Zhang, C.; Su, H. Y.; He, R.; Zhang, R. P.; Li, H. L.; Li, Z. Y.; Wu, X. J.; Ma, C.; Zeng, J. Integration of kinetic control and lattice mismatch to synthesize Pd@AuCu core-shell planar tetrapods with size-dependent optical properties. *Nano Lett.* **2016**, *16*, 3036−3041.
(44) Qi, Y.; Hu, Y.; Xie, M.; Xing, D.; Gu, H. Adsorption of aniline on silver mirror studied by surface-enhanced Raman scattering spectroscopy and density functional theory calculations. *J. Raman Spectrosc.* **2011**, *42*, 1287−1293.
(45) Xia, L. X.; Ma, C. Q.; Wang, J.; Wu, S. W.; Liu, Y.; Zhang, Q.; Song, P. A new strategy for effective distance regulation of the surface plasmon assisted coupling reaction of p-nitrothiophenol to p, p′-dimercaptoazobenzene. *Chem. Commun.* **2017**, *53*, 9582−9585.

https://doi.org/10.1021/acsomega.1c05746
ACS Omega 2022, 7, 1165−1172